

Dual-path state reconstruction scheme for propagating quantum microwaves and detector noise tomography

E. P. Menzel,^{1,2,*} F. Deppe,^{1,2} M. Mariani,^{1,2,†} M. Á. Araque Caballero,^{1,2}
A. Baust,^{1,2} T. Niemczyk,^{1,2} E. Hoffmann,^{1,2} A. Marx,¹ E. Solano,^{3,4} and R. Gross^{1,2}

¹*Walther-Meißner-Institut, Bayerische Akademie
der Wissenschaften, D-85748 Garching, Germany*

²*Physik-Department, Technische Universität München, D-85748 Garching, Germany*

³*Departamento de Química Física, Universidad del País Vasco -
Euskal Herriko Unibertsitatea, Apdo. 644, 48080 Bilbao, Spain*

⁴*IKERBASQUE, Basque Foundation for Science, 48011 Bilbao, Spain*

(Dated: October 11, 2018)

Abstract

Quantum state reconstruction involves measurement devices that are usually described by idealized models, but not known in full detail in experiments. For weak propagating microwaves, the detection process requires linear amplifiers which obscure the signal with random noise. Here, we introduce a theory which nevertheless allows one to use these devices for measuring all quadrature moments of propagating quantum microwaves based on cross-correlations from a dual-path amplification setup. Simultaneously, the detector noise properties are determined, allowing for tomography. We demonstrate the feasibility of our novel concept by proof-of-principle experiments with classical mixtures of weak coherent microwaves.

PACS numbers: 03.65.Wj,07.57.Kp

The reconstruction of the Wigner function [1] or density matrix of a propagating quantum field represents a cornerstone in quantum optical measurement theory and experiments. In quantum homodyne tomography [1, 2], for example, the signal is combined with a local oscillator in a beam splitter, and the intensities at the output ports are subtracted to produce the measurement of the amplified field quadratures in terms of a histogram. The latter gives access to all quadrature moments, or, equivalently, the Wigner function [1]. In this procedure, it is of utmost importance that field amplifiers are not needed in the optical domain because photodetectors with sufficient efficiency are available at the single-photon level [1]. In contrast, in the 1–10 GHz range, which has become highly relevant due to the advent of circuit quantum electrodynamics (QED) [3–11], only theoretical proposals exist for the detection of propagating single microwave photons [12–14]. Consequently, the detection of few-photon microwave signals requires linear amplification. Within well-established “off-the-shelf” technology, cryogenic high electron mobility transistor (HEMT) amplifiers lend themselves to this purpose. They offer flat gain over a broad frequency range, but they obscure the signals by adding random noise [15, 16] of 10–20 photons at 5 GHz. Nevertheless, we prove here that it is still possible to measure all quadrature moments of few-photon propagating microwaves in this situation. Furthermore, we show that our proposed reconstruction method also produces a measurement of all quadrature moments of the detector noise. In this sense, moving from a single amplification chain to a dual-path configuration constitutes a step beyond pure state reconstruction and towards the complete calibration of the measurement device, i.e., detector tomography [17]. We note that so far only state reconstruction of the intra-cavity field has been demonstrated in circuit QED [9]. However, quantum states of propagating microwaves themselves can be valuable in quantum information processing [18] and their full reconstruction represents an important open issue.

We first develop a theory for the measurement of all moments of both a propagating quantum microwave signal and the noise added by the detector. The basic idea is illustrated in Fig. 1a. A signal $S\sqrt{2}$ is equally split at low temperatures by means of a four-port 50-50 microwave beam splitter. The outputs are amplified and synchronously digitized. During this process, the amplifiers add the independent noise contributions χ_1 and χ_2 to the split signals in the detection chains 1 and 2, respectively. Assuming a 180° hybrid ring [19] as a beam splitter (cf. appendix), the recorded time traces are $C_1 = G(S+V+\chi_1)$ and $C_2 = G(-S+V+\chi_2)$, where G is the gain and V represents the ancilla state present in

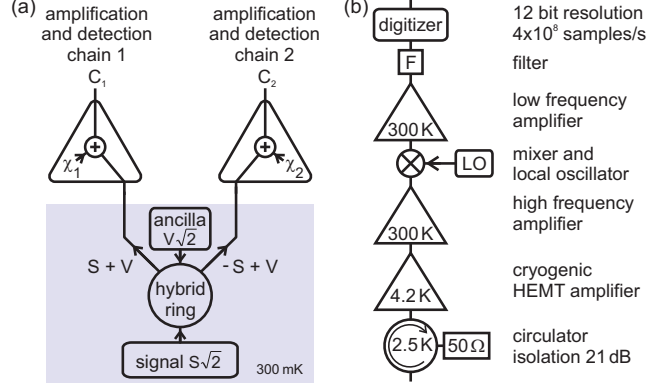


Figure 1: (a) Schematics of the dual path amplification and detection setup. The ancilla port of the 180° hybrid ring is terminated by a $50\ \Omega$ load at $T = 300\text{ mK}$. The split signals are amplified and detected in separate chains, which add the noise χ_1 and χ_2 to the signal. (b) Amplification and detection chain. The noise temperature is dominated by the cryogenic amplifiers anchored at 4.2 K . The isolation of the hybrid ring (40 dB) and the circulator prevents correlated noise contributions from the two chains. The phase difference between C_1 and C_2 is close to 180° .

the fourth port of the hybrid ring. Since we assume full knowledge of V , an obvious choice is the vacuum or, as in this work, a weak thermal state. Vacuum or thermal states at gigahertz frequencies can be prepared reliably in an experiment by controlling the temperature [20, 21]. In the next step, we compute suitable correlations of the form $\langle C_1^\ell C_2^m \rangle$, where $\ell, m \in \mathbb{N}_0$ and the brackets denote ensemble averaging. In contrast to Hanbury Brown and Twiss experiments based on intensity (power) correlations [20], our method is devoted to the correlations of field quadratures (voltages). For the first signal moment, the mean values $\langle \chi_1 \rangle$ and $\langle \chi_2 \rangle$ vanish and one obtains $\langle S \rangle = \langle C_1 \rangle / G = -\langle C_2 \rangle / G$. All higher moments of signal and noise can now be calculated by induction:

$$\begin{aligned}
\langle S^n \rangle &= -\langle C_1^{n-1} C_2 \rangle / G^n \\
&- \sum_{k=1}^{n-1} \sum_{j=0}^k \binom{n-1}{k} \binom{k}{j} \langle S^{n-k} \rangle \langle V^j \rangle \langle \chi_1^{k-j} \rangle \\
&+ \sum_{k=0}^{n-1} \sum_{j=0}^k \binom{n-1}{k} \binom{k}{j} \langle S^{n-k-1} \rangle \langle V^{j+1} \rangle \langle \chi_1^{k-j} \rangle,
\end{aligned} \tag{1}$$

$$\begin{aligned} \langle \chi_1^n \rangle &= + \langle C_1^n \rangle / G^n \\ &\quad - \sum_{k=1}^n \sum_{j=0}^k \binom{n}{k} \binom{k}{j} \langle \chi_1^{n-k} \rangle \langle S^{k-j} \rangle \langle V^j \rangle, \end{aligned} \quad (2)$$

$$\begin{aligned} \langle \chi_2^n \rangle &= + \langle C_2^n \rangle / G^n \\ &\quad - \sum_{k=1}^n \sum_{j=0}^k \binom{n}{k} \binom{k}{j} (-1)^{k-j} \langle \chi_2^{n-k} \rangle \langle S^{k-j} \rangle \langle V^j \rangle. \end{aligned} \quad (3)$$

We note that our conjectures of equal gain in both chains and a perfect 180° hybrid ring are not a restriction in practice. In the derivation of the above formulas, the mutual statistical independence of S , V , χ_1 and χ_2 is crucial because it implies $\langle S^\beta V^\gamma \chi_1^\delta \chi_2^\epsilon \rangle = \langle S^\beta \rangle \langle V^\gamma \rangle \langle \chi_1^\delta \rangle \langle \chi_2^\epsilon \rangle$ for $\beta, \gamma, \delta, \epsilon \in \mathbb{N}_0$. The latter formula also shows that Eqs. (1)-(3) are suitable for quantum signals, where S , V , χ_1 , and χ_2 have to be interpreted as operators.

Explicit expressions for moments of signal and detector noise can be calculated in the spirit of Eqs. (1)–(3). We assume $\langle V^{2j+1} \rangle = 0$ ($j \in \mathbb{N}$) for the ancilla as, e.g., in the case of Gaussian statistics. We note that for the initial correlation $\langle C_1^\ell C_2^m \rangle$ other choices than $\ell = n-1$ and $m = 1$ are possible, as long as $\ell + m = n$ and $\ell, m \in \mathbb{N}$. Typically, balanced products with $\ell \approx m$ result in simpler expressions because of higher symmetry. Starting from $\langle C_1 C_2 \rangle$, $\langle C_1^2 C_2 \rangle$, $\langle C_1^2 C_2^2 \rangle$ we obtain:

$$\begin{aligned} G \langle S \rangle &= \langle C_1 \rangle = -\langle C_2 \rangle \\ G^2 \langle S^2 \rangle &= -\langle C_1 C_2 \rangle + G^2 \langle V^2 \rangle \\ G^3 \langle S^3 \rangle &= -\langle C_1^2 C_2 \rangle - \langle C_1 \rangle (\langle C_1^2 \rangle + \langle C_1 C_2 \rangle - 3G^2 \langle V^2 \rangle) \\ G^4 \langle S^4 \rangle &= -G^4 \langle V^4 \rangle - 6G^2 \langle V^2 \rangle \langle C_1 C_2 \rangle + 6G^4 \langle V^2 \rangle^2 \\ &\quad + \langle C_1 C_2 \rangle^2 + \langle C_1^2 C_2^2 \rangle - \langle C_1^2 \rangle \langle C_2^2 \rangle \end{aligned}$$

$$\begin{aligned} \langle \chi_1 \rangle &\equiv 0 \\ G^2 \langle \chi_1^2 \rangle &= \langle C_1^2 \rangle + \langle C_1 C_2 \rangle - 2G^2 \langle V^2 \rangle \\ G^3 \langle \chi_1^3 \rangle &= \langle C_1^3 \rangle + \langle C_1^2 C_2 \rangle - 2\langle C_1 \rangle (\langle C_1^2 \rangle + \langle C_1 C_2 \rangle) \end{aligned}$$

$$\begin{aligned}
G^4 \langle \chi_1^4 \rangle &= \langle C_1^4 \rangle - 12G^2 \langle V^2 \rangle \langle C_1 C_2 \rangle - 12G^2 \langle V^2 \rangle \langle C_1^2 \rangle \\
&\quad + 6 \langle C_1 C_2 \rangle \langle C_1^2 \rangle + 5 \langle C_1 C_2 \rangle^2 + 12G^4 \langle V^2 \rangle^2 \\
&\quad - 4 \langle C_1 \rangle \langle C_1^3 \rangle - 4 \langle C_1 \rangle \langle C_1^2 C_2 \rangle + 8 \langle C_1 \rangle^2 \langle C_1^2 \rangle \\
&\quad + 8 \langle C_1 \rangle^2 \langle C_1 C_2 \rangle - \langle C_1^2 C_2^2 \rangle + \langle C_1^2 \rangle \langle C_2^2 \rangle
\end{aligned}$$

Similar formulas can be derived for χ_2 . Furthermore, we assume the first moment of the detector noise to vanish for both chains throughout the experimental part of this work. Practically, this implies an offset correction (c.f. appendix). Finally, from Eqs. (1)–(3), the central moments can be retrieved with the binomial transformation

$$\langle (S - \langle S \rangle)^n \rangle = \sum_{k=0}^n \binom{n}{k} (-1)^{n-k} \langle S^k \rangle \langle S \rangle^{n-k}. \quad (4)$$

We emphasize the practical relevance of the above theory by conducting proof-of-principle experiments with weak classical microwaves. The setup is shown in Fig. 1. As signals, we use pulsed coherent microwaves with a frequency of 5.85 GHz generated by a source at room temperature. A series of cold attenuators ensures that the thermal noise at the signal port of the hybrid ring is restricted to that of an effective 50 Ω -termination at the base temperature of 300 mK. The source power at the input of the hybrid ring, P_{in} , is related to an equivalent number of signal photons on average (poa) as described in the appendix. Figure 2a shows the ensemble average of a typical signal used in our experiments. The pulse duration of 1 μs mimics standard cavity decay times in circuit QED experiments [10, 22]. We first demonstrate the suppression of the amplifier noise via cross-correlations. The auto-variance $\langle C_1^2 \rangle - \langle C_1 \rangle^2$ of the ensemble is depicted in Fig. 2b, where one immediately notices the large offset of $35.7 \times 10^{-3} \text{ V}^2$ due to the amplifier noise. In the cross-variance $\langle C_1 C_2 \rangle - \langle C_1 \rangle \langle C_2 \rangle$, this offset is efficiently suppressed by two orders of magnitude. As expected for a coherent signal, the variances are flat and do not allow to distinguish between the “on”- and “off”-regions of the pulses. The fluctuations of the variance signals are smaller for the cross-correlation than for the auto-correlation by a factor of 1.6, see Fig. 2c. Next, we prove that our method works efficiently at the quantum level, i.e., for signals of few photons on average. To this end, we investigate the resolution limits of the constituents of the variance, mean value and cross-product. In Fig. 2d, the root mean square power inside the pulse region is plotted against the signal power at the input of the hybrid ring. We find a large dynamic range of the mean value extending over six decades down to 0.001 poa. This means that

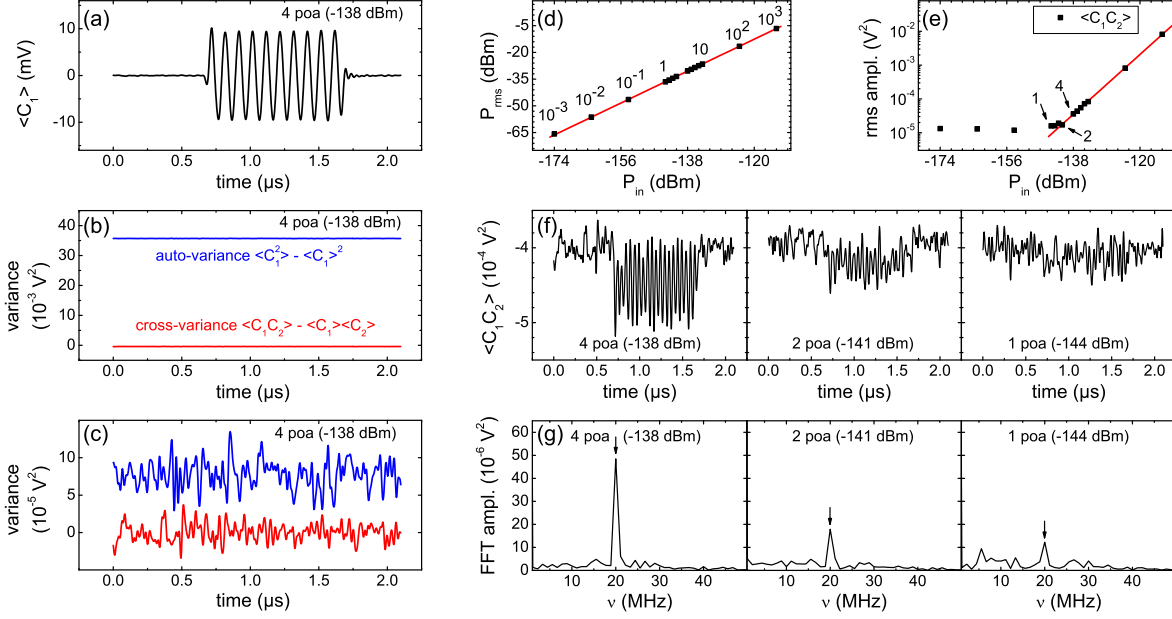


Figure 2: Detection of coherent microwave probing pulses (10^7 traces averaged): (a) Mean value of down converted signal (10 MHz). (b) Auto- (blue) and cross-variance (red). (c) Fluctuations of the auto- and cross-variance. The traces are obtained by subtracting the respective time averages, and the auto-variance trace has been shifted by $8 \times 10^{-5} \text{ V}^2$, for clarity. (d) Dynamic range of the mean value. P_{rms} is the root mean square (rms) power at the digitizer. The numbers above the data points indicate the number of photons on average. (e) Dynamic range of the cross-product $\langle C_1 C_2 \rangle$. The arrows indicate the values obtained from the time traces shown in (f). The rms amplitude inside the pulse region is calculated after subtracting the time average from each data point. (f) Power dependence of the cross-product time traces in the limit of few photons on average. (g) Discrete Fourier transform of the pulse region of the traces shown in (f). The arrows indicate the 20 MHz peaks.

pulse energies as low as $3.7 \times 10^{-26} \text{ J}$ (0.01 poa) are still very well detectable. The power dependence of the cross-product is displayed in Figs. 2e–g. Down to 2 poa, the pulse region is clearly visible (Fig. 2f). For 1 poa, a Fourier transform (Fig. 2g) reveals that the signal component can still be identified. However, the associated peak has approximately the same amplitude as the largest noise peak in the spectrum. Hence, the detection limit of the cross-product (see also Fig. 2e) and therefore the one of the cross-variance is 1–2 poa. We note that this is not a fundamental limit, but is rather due to technical issues such as the

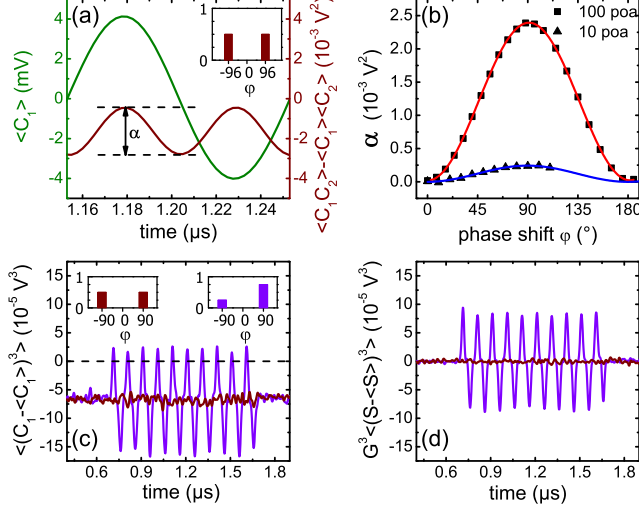


Figure 3: Statistical mixtures of phase-shifted pulses: (a) Mean value and cross-variance. The inset shows the pulse distribution for $\varphi = 96^\circ$. The amplitude α is extracted with a numerical fit. (b) Cross-variance amplitude α plotted versus φ . Squares, 100 poa. Triangles, 10 poa. The solid lines are fits to the data. (c) Third central moment at 100 poa measured with a single amplification chain. Note that, as expected, the trace is not a simple sine function, but $\propto \sin^3(\omega t)$. The insets show the histograms: equally distributed (brown) and with finite skew (violet). (d) Third central moment measured with the dual path method. The dataset is the same as in (c).

ensemble size, filter bandwidth, or bit resolution of the digitizer card.

So far, we have studied time-independent ensemble variances because $\langle f(t)^2 \rangle - \langle f(t) \rangle^2 = 0$ always holds for deterministic signals. Time-dependent variance signals require statistical mixtures of signals. As a first example, a sequence of coherent microwave pulses with alternating phase shifts $\pm\varphi$ is applied to the input line. This corresponds to a statistical mixture with an equally distributed histogram. The mean value and cross-variance are $A \cos(\varphi) \sin(\omega t)$ and $-\alpha \cos^2(\omega t)$, respectively, where $\alpha = A^2 \sin^2(\varphi)$ is the cross-variance amplitude and $\omega/2\pi = 10$ MHz is the signal frequency after the mixers. The frequency doubling $\cos^2(\omega t) \propto [1 + \cos(2\omega t)]$ is confirmed by the data shown in Fig. 3a. Repeating the experiment for different phase shifts, we reproduce the expected $\sin^2(\varphi)$ -dependence of α for 10 and 100 poa (cf. Fig. 3b).

Studying signal mixtures also allows us to address time-dependent third central moments $\langle (S - \langle S \rangle)^3 \rangle$ and $\langle (\chi_1 - \langle \chi_1 \rangle)^3 \rangle$. They are proportional to the skewness of their associated probability histograms and vanish for Gaussian distributions. In particular, both quantities

are zero for an equally distributed histogram. Hence, to observe an oscillating third central moment a statistical mixture with an asymmetric histogram (cf. inset of Fig. 3c) is required. In the experiment, we again create a train of pulses with 100 poa, but this time 75% of them are shifted by the phase φ and 25% by $-\varphi$. Figure 3c shows the third central moment calculated from the data of a single amplification chain. In contrast to the case of an equally distributed mixture, a clear oscillating signal is visible within the pulse duration for a skewed histogram. However, there is an offset of approximately $-7 \times 10^{-5} \text{ V}^3$. In Fig. 3d, one can see that this offset disappears when also taking into account the data from the second chain and applying the dual-path detection scheme described by Eqs. (1)-(4). Following these equations, we can write down the third central moment of C_1 as the sum of the third central moments of signal, noise, and ancilla state:

$$\begin{aligned} \langle (C_1 - \langle C_1 \rangle)^3 \rangle &= G^3 \langle (S - \langle S \rangle)^3 \rangle + G^3 \langle (\chi_1 - \langle \chi_1 \rangle)^3 \rangle \\ &\quad + G^3 \langle (V - \langle V \rangle)^3 \rangle. \end{aligned}$$

Since $\langle (V - \langle V \rangle)^3 \rangle = 0$ due to the Gaussian statistics of V , it becomes obvious that the offset in Fig. 3c must be $G^3 \langle (\chi_1 - \langle \chi_1 \rangle)^3 \rangle$. In this sense, the noise of the detection chain shows non-Gaussian statistics. Although the exact origin of the latter inside the detection chain remains unclear, our experiments provide a first confirmation that the dual-path method is indeed capable of characterizing signal and detector noise moments simultaneously.

In conclusion, we present a method based on off-the-shelf technology and signal recovery techniques to gain access to arbitrary moments of both weak propagating quantum microwaves and the detector noise. In particular, we allow for the use of linear amplifiers adding 10–20 noise photons to the signals. We find that it is crucial to move from a single to two amplification and detection chains and successfully perform proof-of-principle experiments with statistical mixtures of weak pulsed coherent microwaves. We demonstrate sufficient sensitivity for the first two moments and observe indications for a non-Gaussian statistics of the detector noise. The experiments indicate that our dual-path method is a suitable tool for detecting propagating quantum signals such as squeezed states from a Josephson parametric amplifier [23–26], Fock states [9] leaking out of an on-chip resonator [5] or non-classical microwave field states generated in a two-resonator circuit QED setup [7].

Appendix

The ancilla state is assumed to be well known and, hence, its quadrature moments can not be detected by our method. This is not a restriction in practice because vacuum or thermal states at gigahertz frequencies can be prepared reliably in an experiment by controlling the temperature [20, 21]. Furthermore, it is more relevant to characterize quantum states such as Fock states, where part of the Wigner function is negative.

Beam splitter types for the dual-path method. Although in this work we always assume a 180° hybrid ring as beam splitter, other choices are possible, as long as they provide enough isolation between the output ports. However, one has to keep in mind that all lossless, matched and reciprocal beam splitters must be four port devices [19]. Sometimes, as in the case of the Wilkinson power divider [19, 21], the fourth port may be hidden internally and therefore complicate the analytical treatment of the ancilla state. Nevertheless, the equivalent of Eqs. (1)–(3) of the supplemented paper can in principle be calculated for any beam splitter.

Offset correction. The raw data is divided into segments of 4128 traces equivalent to 0.5 s measurement time. For each of these segments, the time average is subtracted from each data point before any other manipulation. Effectively, this procedure acts as a high-pass filter eliminating slow drifts in the data.

The calibration of the input line can be performed *in situ* in our setup. To this end, the $50\ \Omega$ load at the ancilla port of the hybrid ring is temperature controlled using a heater and a thermometer. Except for small deviations, we can assume the hybrid ring, ancilla load, and effective $50\ \Omega$ load at the signal port to have the same temperature. Both loads inject thermal voltage fluctuations into the hybrid ring. The auto-variance of these fluctuations follows the well-known Planck function. Knowing the bandwidth of our setup from measurements with a spectrum analyzer (51 MHz), the gains of the amplification and detection chains are inferred from a numerical fit of the Planck function to the auto-variance data [21]. We find gains of approximately 110 dB for both chains, where small residual gain asymmetries have been absorbed in a compensation factor already. Together with the 0.5 dB loss of the hybrid ring and the total transmission from source to digitizer, we can extract an input line attenuation of 94 dB. From this, we determine the signal power P_{in} at the input of the hybrid ring. The corresponding number of photons on average is the pulse energy $P_{\text{in}}T_{\text{pulse}}$ divided by

the energy quantum $h \times 5.85$ GHz. Here, h is the Planck constant and $T_{\text{pulse}} = 1 \mu\text{s}$ the pulse duration.

* Electronic address: Edwin.Menzel@wmi.badw-muenchen.de

† Present address: Department of Physics, University of California, Santa Barbara, California 93106, USA

- [1] U. Leonhardt, *Measuring the Quantum State of Light* (Cambridge University Press, Cambridge, 1997).
- [2] A. I. Lvovsky and M. G. Raymer, *Rev. Mod. Phys.* **81**, 299 (2009).
- [3] A. Wallraff, et al., *Nature* **431**, 162 (2004).
- [4] A. Blais, R.-S. Huang, A. Wallraff, S. M. Girvin, and R. J. Schoelkopf, *Phys. Rev. A* **69**, 062320 (2004).
- [5] A. A. Houck, et al., *Nature* **449**, 328 (2007).
- [6] F. Deppe, et al., *Nature Physics* **4**, 686 (2008).
- [7] M. Mariantoni, et al., *Phys. Rev. B* **78**, 104508 (2008).
- [8] J. M. Fink, et al., *Phys. Rev. Lett.* **103**, 083601 (2009).
- [9] M. Hofheinz, et al., *Nature* **459**, 546 (2009).
- [10] T. Niemczyk, et al., *Supercond. Sci. Technol.* **22**, 034009 (2009).
- [11] O. Astafiev, et al., *Science* **327**, 840 (2010).
- [12] F. Helmer, M. Mariantoni, E. Solano, and F. Marquardt, *Phys. Rev. A* **79**, 052115 (2009).
- [13] G. Romero, J. J. García-Ripoll, and E. Solano, *Phys. Rev. Lett.* **102**, 173602 (2009).
- [14] G. Romero, J. J. García-Ripoll, and E. Solano, *Phys. Scr.* **T137**, 014004 (2009).
- [15] C. M. Caves, *Phys. Rev. D.* **26**, 1817 (1982).
- [16] A. A. Clerk, M. H. Devoret, S. M. Girvin, F. Marquardt, and R. J. Schoelkopf, Accepted for publication in *Rev. Mod. Phys.* (2009), <http://arxiv.org/abs/0810.4729v1>.
- [17] J. S. Lundeen, et al., *Nature Physics* **5**, 27 (2009).
- [18] P. Kok, et al., *Rev. Mod. Phys.* **79**, 135 (2007).
- [19] R. E. Collin, *Foundations for Microwave Engineering, 2nd ed.* (Wiley and Sons, New York, 2001).
- [20] J. Gabelli, et al., *Phys. Rev. Lett.* **93**, 056801 (2004).

- [21] M. Mariantoni, et al., *Planck spectroscopy and the quantum noise of microwave beam splitters*, In preparation.
- [22] M. Göppl, et al., *J. Appl. Phys.* **104**, 113904 (2008).
- [23] T. Yamamoto, et al., *Appl. Phys. Lett.* **93**, 042510 (2008).
- [24] M. A. Castellanos-Beltran, K. D. Irwin, G. C. Hilton, L. R. Vale, and K. W. Lehnert, *Nature Physics* **4**, 929 (2008).
- [25] N. Bergeal, et al. (2010), *Nature Physics* doi:10.1038/nphys1516.
- [26] A. M. Zagoskin, E. Il'ichev, M. W. McCutcheon, J. F. Young, and F. Nori, *Phys. Rev. Lett.* **101**, 253602 (2008).

Acknowledgments

We thank C. Probst, K. Neumaier and K. Uhlig for providing their expertise in cryogenic engineering and M. Häberlein and C. Rauh for programming support. Furthermore, we acknowledge financial support by the Deutsche Forschungsgemeinschaft via SFB 631, the German Excellence Initiative via NIM, the European project EuroSQIP, UPV-EHU Grant GIU07/40 and Ministerio de Ciencia e Innovación FIS2009-12773-C02-01.

Author contributions

E.P.M. is responsible for the main contributions regarding the theoretical and experimental results presented in this work. F.D. provided important contributions in theory and experiment. E.P.M. and F.D. prepared the manuscript. M.M. provided valuable input to the initial theoretical ideas and helped during the experiments. E.S. supervised the theoretical aspects of this work. M.A.A.C. and A.B. helped with the experimental setup. T.N. and E.H. contributed to discussions and helped editing the manuscript. A.M. and R.G. supervised the experimental aspects of the project.